NJC

ROYAL SOCIETY OF CHEMISTRY

PAPER

View Article Online
View Journal | View Issue

Cite this: *New J. Chem.*, 2020, **44**, 15281

A novel approach to photoelectrochemical immunoassay for procalcitonin on the basis of SnS_2/CdS†

Mengdi Wang, Xuejing Liu, Hongying Jia, Yuyang Li, Xing Ren, Dan Wu, Huan Wang, Qin Wei* and Huangxian Ju

Received 1st June 2020,
Accepted 14th July 2020

DOI: 10.1039/d0nj02764b

rsc.li/njc

A label-free photoelectrochemical (PEC) immunoassay system based on the one-step synthesis of SnS_2/CdS nanocomposites is successfully constructed for sensitively analyzing procalcitonin (PCT). The one-step synthesis of SnS_2/CdS enables the rapid construction of an immunoassay system and avoids the waste of energy. In the constructed immunoassay system, CdS as a sensitizer for PCT analysis not only enhances the light absorption of SnS_2 as a photocurrent generator but also can accelerate the separation of photosensitive electrons and holes by forming a heterostructure. Under optimum conditions, the energy-saving assay platform based on the enhancement photocurrent response of SnS_2/CdS nanocomposites exhibited an excellent performance in analyzing a series of PCTs with different concentrations in a wide linear range of 0.5 pg mL^{-1} to 100 ng mL^{-1} and the detection limit was 0.17 pg mL^{-1}. In view of the advantages of good selectivity, high sensitivity, and facile preparation procedure, the PEC immunoassay is expected to be a promising analytical platform for rapid analysis of PCT and other biomarkers in clinical medical samples.

1. Introduction

Serum procalcitonin (PCT), a calcitonin propeptide material, is extremely low in healthy human plasma, but its levels are abnormally elevated when severe bacterial, fungal, and parasitic infections and sepsis and multiple organ failure occur, which reflects the activity of the systemic inflammatory response.[1,2] The factors affecting the PCT levels include the size and type of infected organs, the type of bacteria, the degree of inflammation, and the status of immune responses.[3,4] Therefore, monitoring PCT levels has a high clinical value for the auxiliary differential diagnosis, prognosis judgment and efficacy observation of systemic bacterial infection, sepsis and the like. Until now, some reports have involved the analysis of PCT, such as fluorescence assay,[5] lateral flow immunoassay,[6] sandwich-type electrochemical assay,[7] electrochemiluminescence assay,[8] and photoelectrochemical (PEC) assay. Among these test methods, PEC immunoassay has more advantages due to its low cost, simple instrumentation, and good stability.[9] More deeply, it displays an ultra-sensitivity and low background signal on account of the completely disparate forms between the excitation and analysis source.[10]

PEC immunoassay has drawn ever-growing interest because of its attractive strengths in chemical and biological analysis. One of the cores of PEC immunoassay construction is to find photoelectric materials with excellent performance to improve the assay's responsiveness.[11] In recent years, besides traditional PEC materials such as TiO_2,[12,13] CdS,[14] and ZnO,[15,16] novel PEC assaying strategies based on semiconductor nanocomposites have received widespread attention.[17] As the new generation of photoelectric materials, Sn-based nanocomposites have attracted extensive attention due to their high photoelectric conversion efficiency.[18]

SnS_2 has a two-dimensional layered hexagonal lattice structure and is an n-type semiconductor with an indirect bandgap of 2.18 to 2.44 eV.[19] Tin atoms are sandwiched between two closely arranged sulfur atoms and are attached to adjacent sandwich structures by a weak van der Waals force. Such layered SnS_2 structures are widely used in batteries[20] and photocatalysts,[21,22] and also exhibit excellent photoelectric performance. For example, Zuo *et al.* through a hot-injection solution-based process carried out the preparation of ultrathin SnS_2 nanoplates (NPLs) for photoelectrochemical water oxidation;[23] Chen and co-workers synthesised two-dimensional SnS_2 nanosheet arrays to achieve efficient photochemical decomposition of water.[24] Most importantly, compared with some heavy metal materials, it has the advantages of low toxicity, earth-abundance and low-price for immunoassay. However, due to its ultra-thin thickness morphology, SnS_2 reveals a weak light absorption capability,

Key Laboratory of Interfacial Reaction & Sensing Analysis in Universities of Shandong, School of Chemistry and Chemical Engineering, University of Jinan, Jinan 250022, P. R. China. E-mail: sdjndxwq@163.com; Fax: +86 531 82767367; Tel: +86 531 82767872

† Electronic supplementary information (ESI) available. See DOI: 10.1039/d0nj02764b

which significantly affects the photoexcitation process and limits its potential applications in optoelectronic devices.[25] Considering the above facts, some ancillary measures and amplification methods should be employed to improve the light absorption of SnS_2, such as metal element doping,[26,27] morphology control,[28] and carbon material introduction.[29,30] In addition, compounding with other semiconductor materials which can serve as sensitizers is one of the most common and effective methods.[31] Combining the matched band gap semiconductors in a PEC system provides a co-sensitized structure with a step-wise energy level, which results in the rapid transfer of photo-induced charges.[32] CdS is reported as a popular and available sensitizer with a prominent visible-light absorption ability.[33] After combining with CdS, the photogenerated charges in SnS_2 can be effectively separated thereby eliminating the recombination probability of SnS_2, prolonging the electron lifetime, and improving the photoelectric conversion efficiency.[34] Therefore, CdS as a favorable candidate is chosen to study a co-sensitized structure with SnS_2.

In this work, the traditional sensitization methods for modifying the weak photoelectric performance materials that were placed on the electrode with a sensitizer were abandoned.[35] We synthesized the SnS_2/CdS nanocomposites by the one-step hydrothermal method with the characteristics of energy conservation and time-saving, which is compared with the multi-step synthesis method for the reported studies. SnS_2/CdS nanocomposites were utilized as a PEC material in the immunoassay approach for PCT analysis with excellent PEC properties. With the successful modification of thioglycolic acid (TGA) and the activation of 1-ethyl-3-(3-dimethylaminopropyl)carbodiimide hydrochloride (EDC)/*N*-hydroxysuccinimide (NHs), the obtained (SnS_2/CdS)/TGA could bind with PCT antibody by forming –CONH–. After effacing nonspecific binding and blocking the excess active sites with bovine serum albumin (BSA), immune complexes were generated on the modified electrodes by incubation with PCT of different concentrations. Ultimately, a label-free immunoassay system was assembled (Scheme 1) for the further photocurrent measurement. At the same time, the ascorbic acid (AA) contained in the test solution serves as an electron donor, providing electrons to capture photogenic holes, inhibiting electron–hole pair recombination and preventing the photocorrosion of CdS,[36–38] thereby triggering photocurrent amplification of SnS_2/CdS. A larger and more stable photocurrent response can be obtained. The excellent insulation and high steric resistance of the immune complexes hindered the transfer of charge and AA, and significantly affected the photocurrent response value. As a result, the analyzed photocurrent is closely related to the concentration of PCT,[39] and the photocurrent response decreases with the increase of PCT. Hence, the concentration of the analyte can be measured based on the PEC signal. The constructed PEC immunoassay has good stability and high sensitivity, which provides an innovative PEC sensing platform for the analysis of PCT in human serum.

2. Experimental section

2.1. Chemicals and instruments

Tin(IV) chloride pentahydrate ($SnCl_4 \cdot 5H_2O$) was purchased from Macklin Biochemical Co., Ltd (Shanghai, China). Cadmium acetate ($C_4H_6CdO_4 \cdot 2H_2O$) was obtained from Shanghai Runjie Chemical Reagent Co., Ltd. Further details are provided in the ESI.†

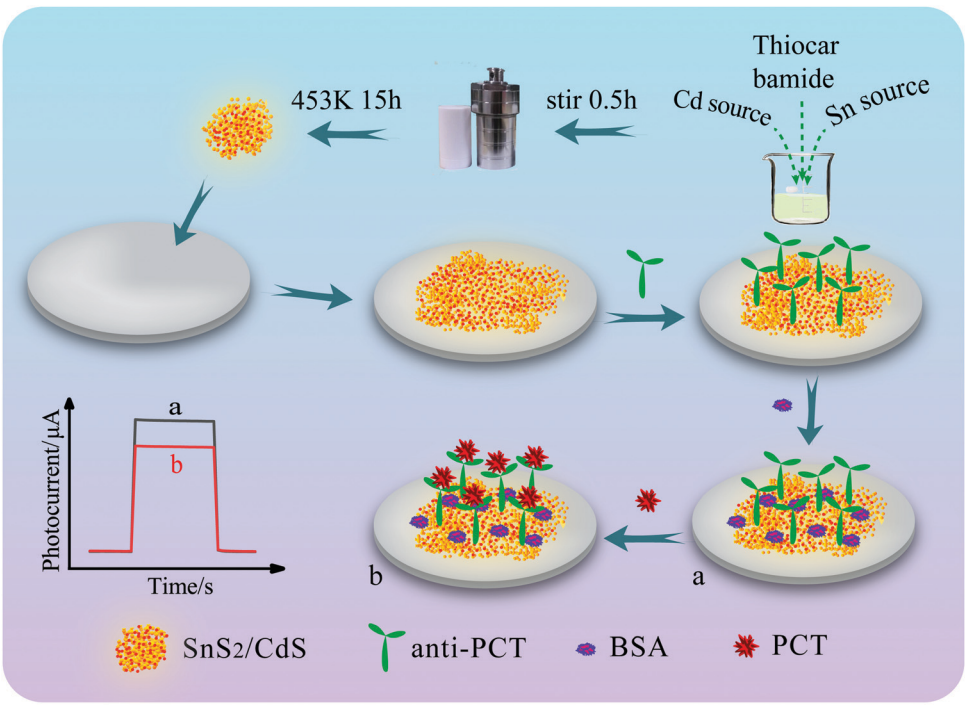

Scheme 1 Schematic diagram of synthesizing SnS_2/CdS and preparing the PEC immunoassay system.

All experiments were performed in accordance with the ''Construction Guidelines of Ethics Review Committees for Clinical Research Involving Human (2019)'', and approved by the ethics committee at ''University of Jinan''. Study participants were fully informed regarding the purposes of the study and consent was obtained.

2.2. Synthesis of SnS_2/CdS nanocomposites

SnS_2/CdS nanocomposites were prepared by a one-step hydrothermal method. The procedure for the synthesis of SnS_2/CdS is as follows: First, 2.6 mmol $C_4H_6CdO_4{\cdot}2H_2O$, 0.9 mmol $SnCl_4{\cdot}5H_2O$, and 6.0 mmol thiocarbamide were successively added into 33 mL of ultra-pure water and stirred for 30 min until the powder was dissolved. The prepared white colloidal solution was then added to a 50 mL Teflon-lined autoclave and heated at 180 °C for 16 h. At the end of the reaction, the reactor was cooled in air until room temperature. After washing and centrifugation, the final product was obtained and dried at 60 °C overnight.

2.3. Preparation of photoelectrochemical immunoassay system

Treatment of the ITO: the size of the ITO glass slices was 2.5 × 1.0 cm^2, and the ITO was washed with each of the following solutions for 30 min sequentially: detergent solution, acetone, ethyl alcohol, and ultra-pure water. After that, the ITO glass was blown dry with nitrogen for later use.

3 mg of SnS_2/CdS powder was accurately weighed and dissolved in 1 mL of ultra-pure water, followed by ultrasonic processing for 10 min. Next, 8 μL of the prepared SnS_2/CdS suspension was dripped onto the ITO electrodes and dried in air. Then, the obtained ITO/(SnS_2/CdS) electrodes were immersed in 3 mmol L^{-1} TGA solution for 30 min and rinsed with ultra-pure water. After that, the modified electrodes were activated with 6 μL of EDC/NHs solution, consisting of 200 mmol L^{-1} EDC and 50 mmol L^{-1} NHs, for 1 h. Following washing, 6 μL of anti-PCT (1 μg mL^{-1}) was cast onto the assembled electrode surface and then incubated at 4 °C for about 1.5 h to immobilize the antibody. The surface of the electrodes was subsequently coated with 6 μL of bovine serum albumin (BSA, 0.1 wt%) to block non-specific active sites, and then the electrodes were dried at 4 °C for about 1 h. After that, 6 μL of PCT with a series of different concentrations were dripped onto the procured above electrodes and then the electrodes were incubated at 4 °C for another 1.5 h to the specific immune binding antigen. After each step, the assembled electrodes were washed with 0.1 mol L^{-1} phosphate buffer solution (PBS, pH 7.4). A label-free PEC immunoassay system was constructed.

2.4. Photoelectrochemical analysis

During PEC analysis, without additional explanation, a three-electrode system was used and 15 mL of PBS (pH 7.4, 0.1 mol L^{-1}) including 0.1 mol L^{-1} AA was employed as the electrolyte. The bias voltage was 0 V, and the wavelength of the light source was 450 nm.

3. Results and discussion

3.1. Characterization of SnS_2/CdS nanocomposites

The crystallization of SnS_2/CdS nanocomposites was analyzed *via* X-ray diffraction (XRD), and their patterns are shown in Fig. 1A. The diffraction peaks appeared at 2θ = 15.0°, 28.2°, 32.1°, 41.9°, 50.0° and 52.5° (pattern b) correspond to the (001), (100), (101), (102), (110) and (111) planes of hexagonal phase SnS_2 (PDF#23-0677), respectively. Compared with pure SnS_2, the XRD pattern of SnS_2/CdS nanocomposites (pattern c) was found with some new diffraction peaks at 2θ = 24.8°, 26.5°, 43.7° and 47.8°, which can be indexed to (100), (002), (110) and (103) planes of hexagonal phase CdS (PDF#41-1049). Besides, the (100) and (111) planes of SnS_2 and the (101) and (112) planes of CdS had near peak positions, which resulted in the wider diffraction peaks. From what has been researched above, the SnS_2/CdS nanocomposites were proved to be prepared successfully.

Moreover, the morphological characterization of the SnS_2/CdS nanocomposites was investigated using a high-resolution transmission electron microscope (HRTEM). As shown in Fig. S1A (ESI†), the hexagonal SnS_2 appeared as nanosheets of about 50 nm, and the CdS appeared as particles of about 5 nm (Fig. S1B, ESI†). After the hydrothermal reaction, as displayed in Fig. 1B, the as-synthesized materials were nanoparticles with a size of about 5 nm. Furthermore, the lattice fringes of 0.278 nm and 0.355 nm are respectively attributed to the (101) plane of SnS_2 and the (100) plane of CdS. The change in the morphology of SnS_2 further confirmed the successful compounding of materials.

To characterize the chemical composition of SnS_2/CdS, the material was analyzed by X-ray photoelectron spectroscopy (XPS). The XPS survey analysis (Fig. 3C) indicates that the as-prepared nanocomposites are mainly composed of Sn, Cd and S elements. Their homologous photoelectron peaks are Sn 3d, Cd 3d, and S 2p, respectively. The high-resolution XPS spectrum of Sn (Fig. S2A, ESI†) exhibits two peaks $3d_{5/2}$ and $3d_{3/2}$ at 486.7 eV and 495.0 eV respectively, which can be arising from Sn^{4+} in SnS_2.[40] In Fig. S2B (ESI†), the binding energy values of 405.0 eV and 411.1 eV are assigned to Cd $3d_{3/2}$ and Cd $3d_{5/2}$ of CdS according to the literature. In Fig. S2C (ESI†), the spectrum has been fitted by considering with a spin–orbit splitting of 0.9 eV between $2p_{3/2}$ and $2p_{1/2}$. The two peaks at 161.2 eV and 162.3 eV are consistent with the reported values of S^{2-}. The elemental composition of the prepared material can be further determined by energy dispersive spectroscopy (EDS).[41] Fig. 1D further confirmed that the Sn, Cd, and S existed. The above results proved that the SnS_2/CdS nanocomposites were prepared successfully.

3.2. Photogenerated charge-transfer mechanism of SnS_2/CdS materials

Under the conditions of visible light irradiation, the photogenerated charge-transfer process of SnS_2/CdS nanocomposites is discussed in this chapter. Fig. 2A shows that the photocurrent response of SnS_2/CdS nanocomposites (curve a) was significantly

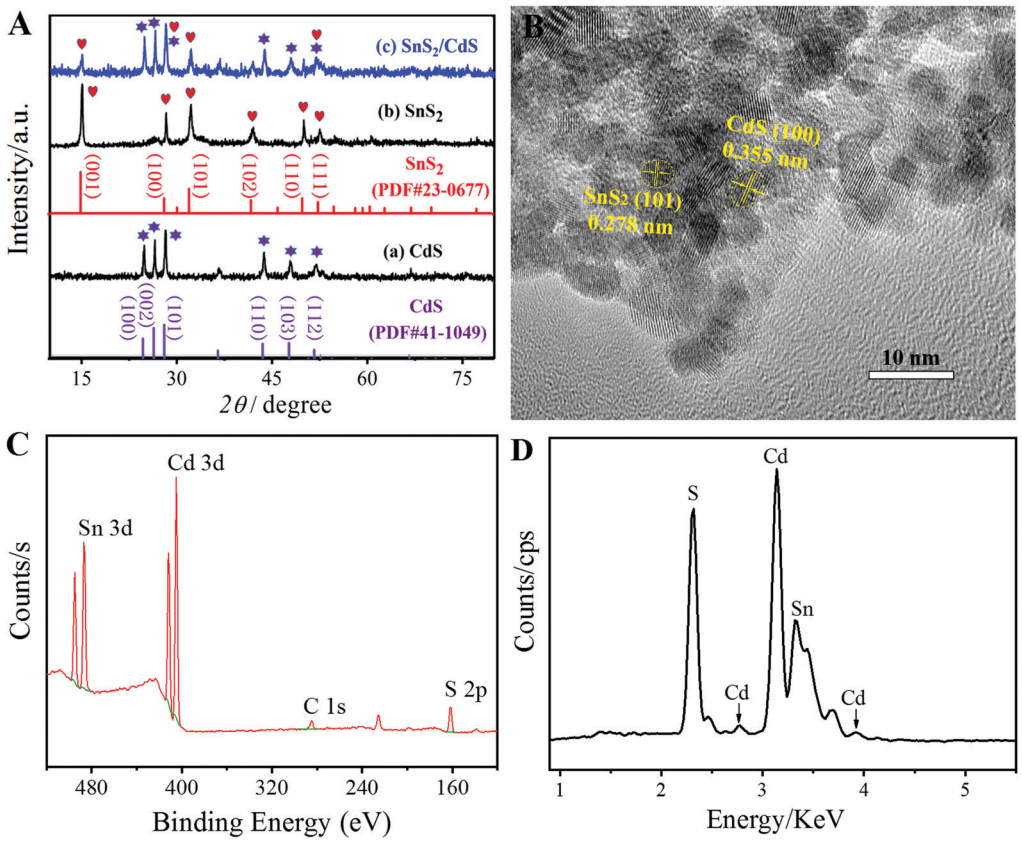

Fig. 1 (A) XRD pattern of (a) CdS, (b) SnS_2, and (c) SnS_2/CdS; (B) HRTEM images of SnS_2/CdS; (C) typical XPS survey spectrum of SnS_2/CdS; (D) EDS pattern of SnS_2/CdS.

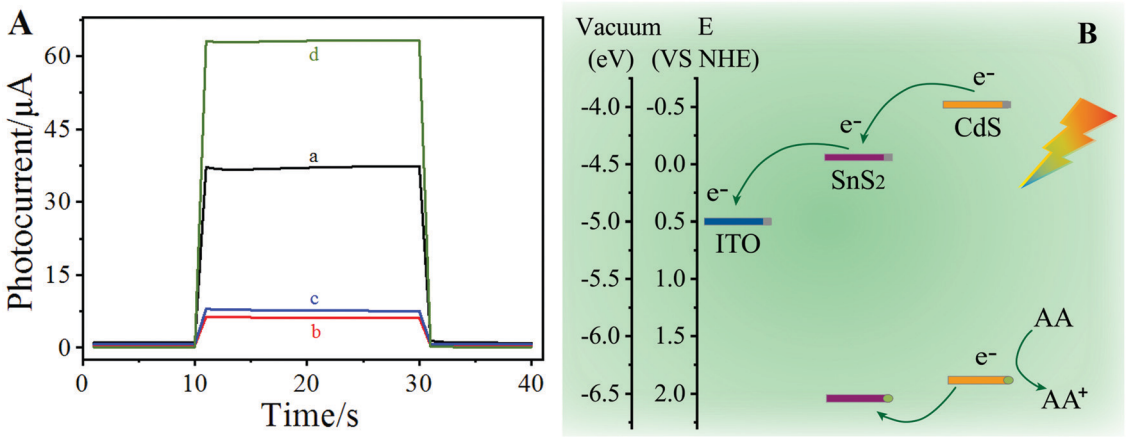

Fig. 2 (A) Time-based photocurrent response curves of (a) SnS_2/CdS, (b) CdS, (c) SnS_2 and (d) SnS_2/CdS (under optimal conditions); (B) photogenerated charge transfer process of SnS_2/CdS.

higher than that of CdS (curve b) and SnS_2 (curve c). On the basis of the experimental results and the band matching theory, the charge transfer mechanism of SnS_2/CdS for amplifying the PEC signal was extrapolated. The conduction band (CB) edge positions of SnS_2 and CdS are −0.06 eV and −0.52 eV (*vs.* NHE) respectively that show a ladder-shaped pattern. Therefore, photoelectrons can be transferred rapidly from the CB of CdS to that of SnS_2, which will deeply reduce the recombination rate of photogenerated electron–hole pairs. In addition, the work function of ITO is −5 eV, more negative than the CB of SnS_2. This situation facilitates the transfer of electrons from the CB of SnS_2 to the electrode. Meanwhile, the photogenerated holes move from the valence band of SnS_2 to that of CdS and are captured by AA in solution, thereby generating a larger photocurrent. Thus, the electrode modified by the SnS_2/CdS nanocomposites has a larger photocurrent signal than its two pure components (SnS_2 and CdS).

3.3. Characterization of the fabricated PEC immunoassay system

Electrochemical impedance spectroscopy (EIS) is an effective method to monitor the fabrication of a PEC immunoassay system.[42] As demonstrated in Fig. 3A, two parts make up the complete EIS spectrum: one is the high-frequency sub-region, which is related to the charge transfer process and is shown as a semicircle; the other is the low-frequency sub-region that appears as the linear part and indicates a diffusional limiting step of the electrodes. The semicircular diameter is a considerable assignment in characterizing the change of electrode interfacial performance. Fig. 3A shows that the bare ITO electrode (curve a) has a diminutive resistance, which manifested that the surface oxidation resistance of the conductive glass is very low.[43] After the modification with SnS_2/CdS photoactive materials, the semicircular diameter had a small increase (curve b) on account of the relatively poor conductivity of the semiconductor. The constant modification of TGA and EDC/NHs has little hindrance to the transfer of interface electrons, so the impedance value (curve c) increases but changes little. Then, after antibody binding (curve d), BSA clogging (curve e) and antigen-specific adsorption (curve f), the impedance value increases in turn and changes more than before. This result can be explained by the fact that the formed protein layer serving as a non-electroactive molecule obviously inhibited the diffusion of ferricyanide and restrained electron's transport between ferricyanide and the electrode surface. The gradual increase of impedance demonstrated the successful formation of the PEC immunoassay system.

Meanwhile, the monitoring of the manufacturing process of the PEC immunoassay system can also be applied to the effective method of photocurrent response measurement. Fig. 3B shows that the photocurrent response value of the ITO/(SnS_2/CdS) (curve b) is significantly larger than that of the bare ITO (curve a), suggesting the outstanding performance of the photoactive substrate material of PEC immunoassay. The subsequent modification with TGA and EDC/NHs made the photocurrent response decrease (curve c) because the modification of above materials hindered the transfer of the interface electron. The photocurrent response values continue to gradually decrease with the anti-PCT binding, BSA sealing, and PCT specific anchoring (curve d–f), which is because the protein steric hindrance severely impeded the electron transfer and weakened the response value. The above experimental results further proved the successful construction of the proposed PEC immunoassay system.

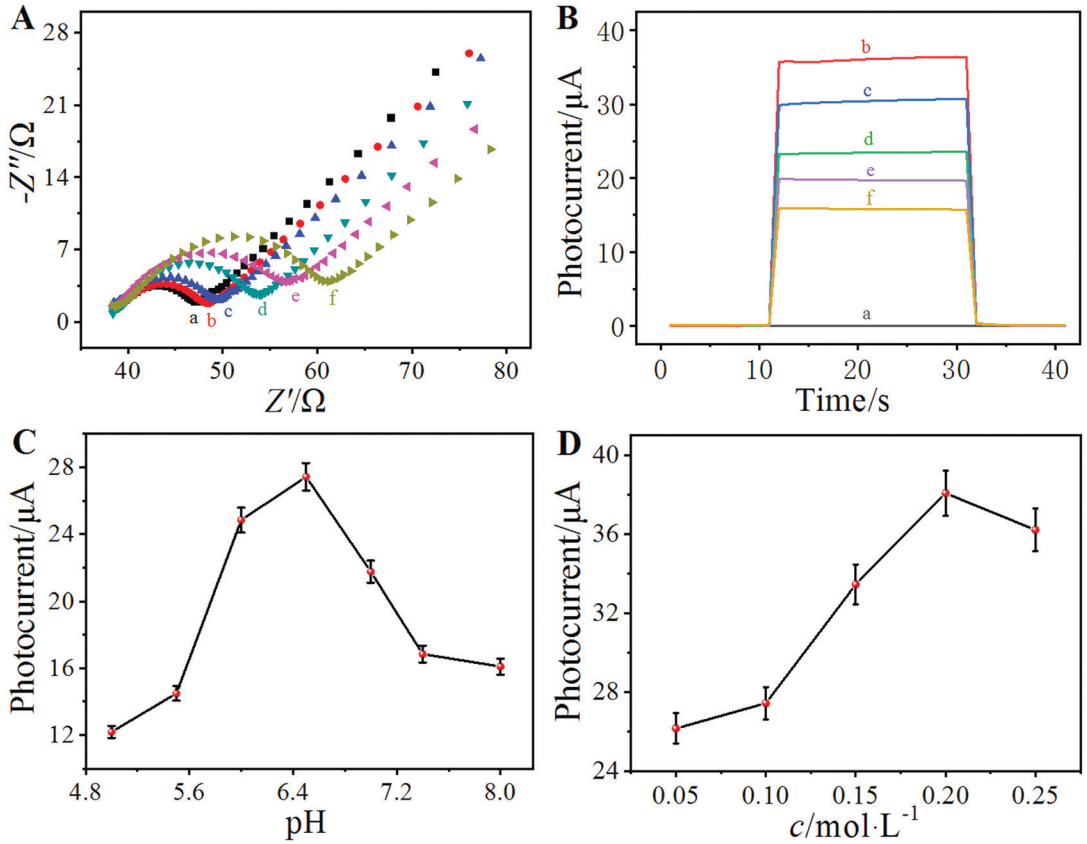

Fig. 3 (A) EIS Nyquist plots and (B) time-based photocurrent response curves of: (a) ITO, (b) ITO/(SnS_2/CdS), (c) ITO/(SnS_2/CdS)/(EDC/NHs), (d) ITO/(SnS_2/CdS)/(EDC/NHs)/anti-PCT, (e) ITO/(SnS_2/CdS)/(EDC/NHs)/anti-PCT/BSA, (f) ITO/(SnS_2/CdS)/(EDC/NHs)/anti-PCT/BSA/PCT. The substrate solution of EIS spectra was 2.5 mmol L^{-1} $[Fe(CN)_6]^{3-/4-}$ solution including 0.10 mol L^{-1} of KCl. PEC test was accomplished in PBS (0.1 mol L^{-1} pH = 7.4) including 0.1 mol L^{-1} AA as electron donor with 0 V applied potential. Experimental optimization design: The effect of (C) pH and (D) AA concentration on the photocurrent response of the assay. (c_{PCT} = 500 pg mL^{-1}).

3.4. Optimization of analysis conditions

Different pH values and the concentrations of AA have significant effects on the photocurrent responses of the PEC immunoassay. For the purpose of improving the performance of the devised PEC immunoassay, both the pH value and concentration of AA were optimized in this experiment. As shown in Fig. 3C, with the changes in pH values ranging from 5.0 to 6.5 the photocurrent response value augment, and the maximum value was obtained at pH 6.5. Furthermore, it decreased with the increment of pH values from 6.5 to 8.0. Therefore, the pH of 6.5 was selected for the analysis of PCT. Fig. 3D shows that with the gradual increment of the AA concentration, the photocurrent response value increased and peaked at 0.2 mol L^{-1}, and then began to decrease. Hence, the AA concentration selected during the next immunoassay analysis process was 0.2 mol L^{-1}.

3.5. Analysis of PCT

In this work, by analyzing the PEC signals of electrodes modified with different concentrations of PCT, under the optimum conditions, the photocurrent curves were obtained for the characterization of PEC behavior. As depicted in Fig. 4A, the photocurrent values of the PEC immunoassay varied with different concentrations of PCT. With the decreasing concentration of the analytes, the photocurrent response value gradually increased. The photocurrent response value of the constructed electrode has a good linear relationship with the logarithm of the modified PCT concentration ranging from 0.5 pg mL^{-1} to 100 ng mL^{-1} (Fig. S3A, ESI†). The change of photocurrent intensity before and after the modification of PCT is fitted with the logarithm of the modified PCT concentration (Fig. 4B), and the equation is $\Delta I = 26.18 + 5.95 \lg c$, in which the correlation coefficient was 0.9963 and the detection limit was 0.17 pg mL^{-1}. Table S1 (ESI†) shows a comparison of the PCT linear range and analysis limit between our proposed PEC immunoassay and other reported analysis methods.

3.6. Stability, selectivity, and reproducibility

Stability is a principal element, which could affect the application of immunoassays. To investigate the stability of the immunoassay system, the photocurrent response of the immunoassay has to be tested under reduplicative on/off irradiation cycles. Under incubation of 0.5 ng mL^{-1} of PCT, the excitation light source was cycled at 20 second intervals of on and off for 15 cycles. As shown in Fig. 4C, the photocurrent response was stable with no obvious fluctuations and the relative standard deviation (RSD) was 0.87%, which proved that the immunoassay has good stability.

In order to appraise the selectivity of the constructed immunoassay system, interference analysis was performed by adding some representative interfering substances such as alpha-fetoprotein (AFP),

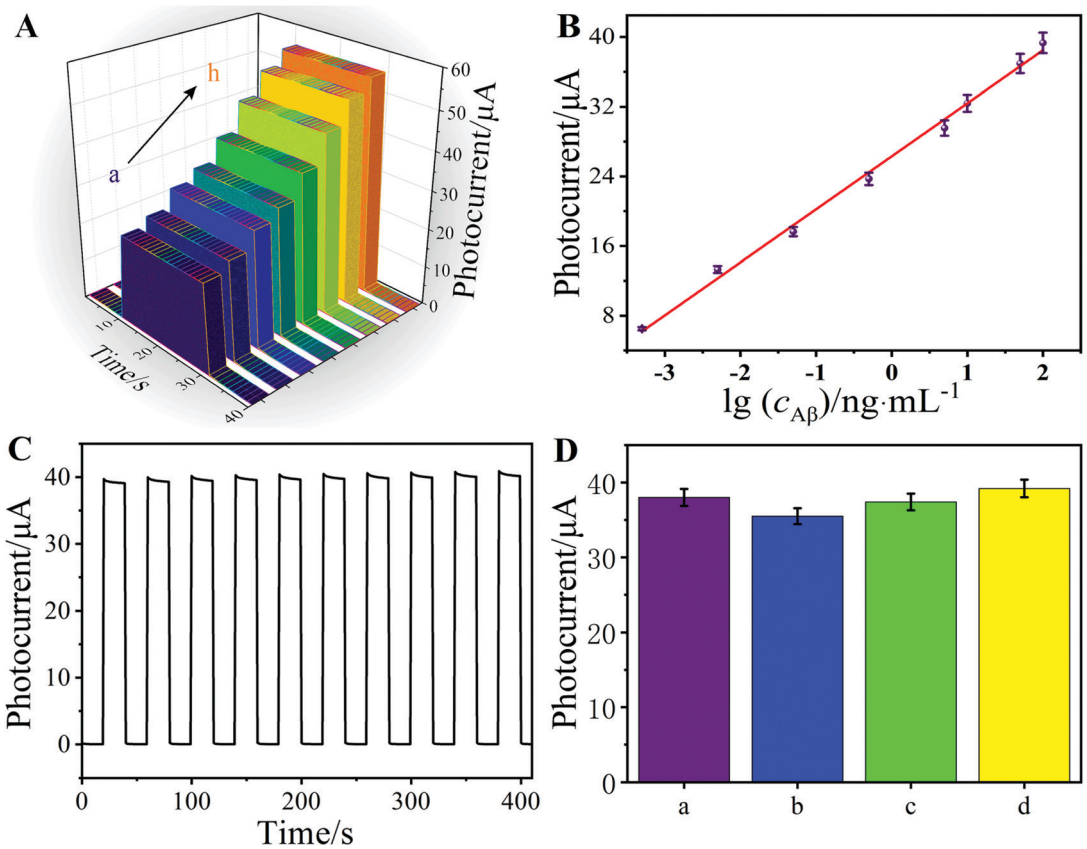

Fig. 4 (A) Photocurrent response values and (B) calibration curves of current intensity before and after PCT modification at different concentrations. (C) Under 15 on/off irradiation cycles, time-based photocurrent responses of the PEC immunoassay, PCT 0.5 ng mL^{-1}. (D) Selectivity of the PEC immunoassay: (a) 0.5 ng mL^{-1} PCT, (b) 0.5 ng mL^{-1} PCT + 50 ng mL^{-1} AFP, (c) 0.5 ng mL^{-1} PCT + 50 ng mL^{-1} CEA, (d) 0.5 ng mL^{-1} PCT + 50 ng mL^{-1} BSA, (e) 0.5 ng mL^{-1} PCT + 50 ng mL^{-1} MAPT. Error bars = SD (n = 3).

carcinoembryonic antigen 125 (CEA), bovine serum albumin (BSA), and microtubule-associated protein tau (MAPT). The photocurrent response of 0.5 ng mL^{-1} PCT solution including 50 ng mL^{-1} different interfering substances was analyzed, respectively. Fig. 4D shows that the presence of the interfering substance could not cause an evident change in the photocurrent response of the assay (RSD = 3.3%), which validated that the immunoassay has satisfactory selectivity for PCT analysis.

Under the optimum experimental conditions, five electrodes independently modified with 0.5 ng mL^{-1} PCT were used for repetitive testing, and the photocurrent response value showed no significant change, with the RSD less than 3.3% (Fig. S3B, ESI†). The above experimental results demonstrated that the PEC immunoassay exhibits prominent reproducibility.

3.7. Analysis of real samples

For the purpose of verifying the practical applicability of PEC immunoassay, PCT was analyzed in an artificial serum sample through the standard addition method. Table S2 (ESI†) shows that the experimental results of the RSD are 2.8–4.1%, and the recovery rates are 100–102%, which indicate that the as-built immunoassay has high accuracy and precision.

4. Conclusion

In summary, a label-free photoelectrochemical immunoassay system, based on SnS_2/CdS nanocomposites, was constructed for PCT analysis. SnS_2/CdS nanocomposites were synthesized by the one-step hydrothermal method under acidic conditions. The PEC immunoassay system was constructed by a simple layer-by-layer approach. The energy level matching of CdS and SnS_2 promotes the separation of photogenerated charges, prolongs the electron lifetime, reduces the recombination rate of photogenerated charges and enhances the photoelectric conversion efficiency. Consequently, the immunoassay obtained a good linear response in a wide concentration range from 0.5 pg mL^{-1} to 100 ng mL^{-1} and with a detection limit of 0.17 pg mL^{-1}, under the optimum conditions. Meanwhile, the immunoassay exhibited high stability and good sensitivity, which proved to be an excellent analysis method for the analysis of PCT and other biomarkers in clinical diagnosis. Additionally, the PEC immunoassay in this work is still in the early stages and will be further extended to analyze multiple biomarkers synchronously, especially in clinical analysis in the near future.

Conflicts of interest

There are no conflicts to declare.

Acknowledgements

This study was supported by the National Key Scientific Instrument and Equipment Development Project of China (No. 21627809), the National Natural Science Foundation of China (No. 21777056), the Special Foundation for Taishan Scholar Professorship of Shandong Province, Jinan Scientific Research Leader Workshop Project (2018GXRC024, 2018GXRC021), the Innovation Team Project of Colleges and Universities in Jinan (No. 2019GXRC027).

References

1 H. G. Schneider and Q. T. Lam, *Pathology*, 2007, **39**, 383–390; H. G. Schneider and Q. T. Lam, *Pathology*, 2007, **39**, 383–390.
2 S. Harbarth, K. Holeckova, C. Froidevaux, D. Pittet, B. Ricou, G. E. Grau, L. Vadas and J. Pugin, *Am. J. Respir. Crit. Care Med.*, 2001, **164**, 396–402.
3 G. A. Wanner, M. Keel, U. Steckholzer, W. Beier, R. Stocker and W. Ertel, *Crit. Care Med.*, 2000, **28**, 950–957.
4 E. A. Mann, G. L. Wood and C. E. Wade, *Burns*, 2011, **37**, 549–558.
5 D. Rascher, A. Geerlof, E. Kremmer, P. Krämer, M. Schmid, A. Hartmann and M. Rieger, *Biosens. Bioelectron.*, 2014, **59**, 251–258.
6 K. V. Serebrennikova, J. V. Samsonova, A. P. Osipov, D. Senapati and D. V. Kuznetsov, *Nano Hybrids Composites*, 2017, **13**, 47–53.
7 P. Liu, C. Li, R. Zhang, Q. Tang, J. Wei, Y. Lu and P. Shen, *Biosens. Bioelectron.*, 2019, **126**, 543–550.
8 P. Chen, X. Qiao, J. Liu, F. Xia, T. Dong and C. Zhou, *Sens. Actuators, B*, 2018, **B267**(AUG.), 525–532.
9 T. Wu, Y. Zhang, D. Wei, X. Wang, T. Yan, B. Du and Q. Wei, *Sens. Actuators, B*, 2018, **256**, 812–819.
10 W. W. Zhao, J. J. Xu and H. Y. Chen, *Chem. Soc. Rev.*, 2015, **44**, 729–741.
11 H. Yang, H. Chen, L. Cao, H. Wang, W. F. Deng, Y. M. Tan and Q. J. Xie, *Talanta*, 2020, **212**, 8.
12 A. Qileng, C. Yue, W. Jie, H. Lei, W. Liu, S. Zhang and Y. Liu, *Sens. Actuators, B*, 2017, **254**, 727–735.
13 C. Tian, L. Wang, F. Luan and X. Zhuang, *Talanta*, 2019, **191**, 103–108.
14 X. Rui, L. Peng, W. Bin, W. Xueping, P. Xuehui, D. Bin, F. Dawei and W. Qin, *Sens. Actuators, B*, 2018, **274**, 349–355.
15 Z. Liu, W. Yun, W. Bo, Y. Li, Z. Liu, J. Han, K. Guo, Y. Li, T. Cui and H. Li, *Int. J. Hydrogen Energy*, 2013, **38**, 10226–10234.
16 R. Xu, Y. Jiang, L. Xia, T. Zhang, L. Xu, S. Zhang, D. Liu and H. Song, *Biosens. Bioelectron.*, 2015, **74**, 411–417.
17 J. Xi, H. Wang, B. Zhang, F. Zhao and B. Zeng, *Sens. Actuators, B*, 2020, **320**, 128409.
18 J. Mazloom, F. E. Ghodsi and H. Golmojdeh, *J. Alloys Compd.*, 2015, **639**, 393–399.
19 Z. Xing, Z. Qi, G. Lin, H. Li and T. Zhai, *Adv. Funct. Mater.*, 2016, **26**, 4405–4413.
20 J. W. Seo, J. T. Jang, S. W. Park, C. Kim, B. Park and J. Cheon, *Adv. Mater.*, 2010, **20**, 4269–4273.
21 Y. Jing, X. Cheng-Yan, M. Fei-Xiang, H. Sheng-Peng, Z. Yu-Wei and Z. Liang, *ACS Appl. Mater. Interfaces*, 2014, **6**, 22370–22377.
22 M. Hui, T. Wang, H. Chen, Y. Liu, Y. Xiang, Z. Yi and Y. Zhang, *NANO*, 2016, **11**, 1650087.

23 Y. Zuo, Y. P. Liu, J. S. Li, R. F. Du, X. T. Yu, C. C. Xing, T. Zhang, L. Yao, J. Arbiol, J. Llorca, K. Sivula, N. Guijarro and A. Cabot, *ACS Appl. Mater. Interfaces*, 2019, **11**, 6918–6926.
24 L. D. Chen, E. Z. Liu, F. Teng, T. X. Zhang, J. Feng, Y. M. Kou, Q. Sun, J. Fan, X. Y. Hu and H. Miao, *Appl. Surf. Sci.*, 2019, **467**, 698–707.
25 H. Zang, P. K. Routh, Y. Huang, J. S. Chen, E. Sutter, P. Sutter and M. Cotlet, *ACS Nano*, 2016, **10**, 4790–4796.
26 Z. Nan, Y. Min-Quan, T. Zi-Rong and X. Yi-Jun, *ACS Nano*, 2014, **8**, 623–633.
27 P. Ji, M. Takeuchi, T. M. Cuong, J. Zhang, M. Matsuoka and M. Anpo, *Res. Chem. Intermed.*, 2010, **36**, 327–347.
28 X. Chen, L. Wang, C. Renpeng, Y. Hongfei and G. Changzeng, *Nano Res.*, 2017, **10**, 1434–1447.
29 X. G. Ma, Y. H. Lv, J. Xu, Y. F. Liu, R. Q. Zhang and Y. F. Zhu, *J. Phys. Chem. C*, 2012, **116**, 23485–23493.
30 S. U. Khan, M. Alshahry and I. W. Jr, *Science*, 2002, **297**, 2243–2245.
31 C. Tian, L. Wang, F. Luan, X. Fu, X. Zhuang and L. Chen, *Chem. Commun.*, 2019, **55**, 12479–12482.
32 S. J. Hong, S. Lee, J. S. Jang and J. S. Lee, *Energy Environ. Sci.*, 2011, **4**, 1781–1787.
33 R. Xu, D. Wei, B. Du, W. Cao, D. Fan, Y. Zhang, Q. Wei and H. Ju, *Biosens. Bioelectron.*, 2018, **122**, 37–42.
34 Y. Liu, Y. Zhang, D. Wu, D. Fan, X. Pang, Y. Zhang, H. Ma, X. Sun and Q. Wei, *Biosens. Bioelectron.*, 2016, **86**, 301–307.
35 J. Feng, F. Li, X. Li, Y. Wang, D. Fan, B. Du, Y. Li and Q. Wei, *Biosens. Bioelectron.*, 2018, **117**, 773–780.
36 L. Shanshan, C. Huijuan, W. Zhaoyin, T. Wenwen and D. Zhihui, *Chem. Commun.*, 2015, **51**, 14259–14321.
37 H. Yu, X. Huang, P. Wang and J. Yu, *J. Phys. Chem. C*, 2016, **120**, 3722–3730.
38 R. Xu, L. Liu, X. Liu, Y. Li, R. Feng, H. Wang, D. Fan, D. Wu and Q. Wei, *ACS Appl. Mater. Interfaces*, 2020, **12**, 7366–7371.
39 W. W. Zhao, J. J. Xu and H. Y. Chen, *Chem. Soc. Rev.*, 2015, **46**, 729–741.
40 F. Zhang, Y. Chen, W. Zhou, C. Ren, H. Gao and G. Tian, *ACS Appl. Mater. Interfaces*, 2019, **11**, 9093–9101.
41 Y. Qian, J. Feng, D. Fan, Y. Zhang, X. Kuang, H. Wang, Q. Wei and H. Ju, *Biosens. Bioelectron.*, 2019, **131**, 299–306.
42 Y. Xiaoxue, L. Mingshi, H. Ye, W. Zhengguo, W. Yanying, D. Hongping, X. Xiaoxing, L. Chunya and S. Dong, *Sens. Actuators, B*, 2018, **275**, 199–205.
43 R. Xu, R. Feng, D. Wei, T. Yan, Y. Zhang, W. Cao, D. Fan, Q. Wei and H. Ju, *Sens. Actuators, B*, 2019, **301**, 127099.

